Simple Robust Rotor 5 MW Synchronous Reluctance Generator

Jandré Dippenaar and Maarten J. Kamper
Department of Electrical and Electronic Engineering
Stellenbosch University, Stellenbosch, South Africa
jandredippenaar@gmail.com, kamper@sun.ac.za

***Abstract*—In modern synchronous reluctance machines, distributed flux barriers are typically used in the rotor designs. This greatly reduces the mechanical strength and robustness of especially large rotors. In this paper, the capability of simple salient-pole rotor synchronous reluctance generators at a 5 MW power level is investigated. Different salient pole rotor profiles are considered in the finite element design optimisation of the generator. It is found, surprisingly, that with the simple salient pole rotor, similar torque density and efficiency are obtained as in published equivalent distributed flux barrier rotor reluctance synchronous generators.**

***Index Terms*—Wind energy, generators, synchronous reluctance**

I. Introduction

Wind turbines are one of the solutions currently being implemented to address a globally increasing energy demand. Ongoing research, concerning every aspect of a wind turbine, aims to find better solutions in this field. One of these research aspects is the generator. In wind generators, permanent magnet materials are often used because of the good power density and efficiency that are associated with using magnets. However, there is a strong search for non-permanent magnet generator solutions due to the cost, availability and demagnetisation danger of permanent magnets. Non-permanent magnet (non-PM) generators include, amongst others, induction generators, wound-rotor synchronous generators, switched reluctance generators (SRGs), wound-field flux-switching generators (WF-FSGs) and reluctance synchronous generators (RSGs). The conductor-less iron rotor, good efficiency and standard converter make the RSG very attractive to use.

RSGs have especially attracted the attention of researchers at a 5 MW power level [1], [2], [3]. Wind generators have grown in size over the last couple of years, in both offshore and onshore implementations. Onshore turbine offerings by *GE*, *Vestas* and *Siemens Gamesa* have all recently crossed the 5 MW mark, while offshore turbines have crossed the 10 MW mark.

Furthermore, full-rated power converters have become increasingly popular as an interface between the generator and the power grid in systems using wind- and hydro-energy generation [4], [5]. Maximum torque per ampere and adjustable speed can be achieved using these power converters.

Wind generators can be connected to the turbines either directly or via gearboxes. For wind generation, it has been found that the (so-called) medium-speed gearbox generator systems have the highest efficiency. The main reason for this is the fewer stages required in the gearbox. The medium-speed range for wind generators, in general, is taken as 100–500 r/min. The focus of this paper is therefore on the RSG design for a medium-speed wind generator at a 5 MW power level.

In the RSGs of both [1] and [2], typical distributed flux barriers are used in the design of the rotors, which can be seen in Fig. 1. It is interesting how the designs differ. A potential problem in both these designs is the mechanical strength of the rotors. It is shown in [6] that the thin ribs at the end of the rotor flux barriers are especially susceptible to mechanical failure. Assuming mechanical feasibility, as is done in [2], can thus be problematic. This paper removes the complexity of the flux-barrier design process by focusing on a more robust RSG rotor design, as illustrated in Fig. 2. This rotor design is similar to rotors that can be found in some other, non-permanent magnet machines mentioned previously, such as the SRG in [7] and the WF-FSG in [8]. A major difference is that the rotor in this paper is used with a conventional stator winding, similar to [3]. However, where [3] focused on drastically changing a baseline salient-pole RSG into one with ”split poles”, this paper focuses on making a series of subtle changes to a baseline, simple salient-pole

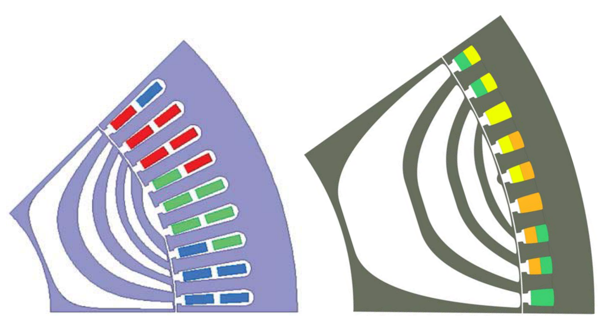
(a) (b)

Fig. 1. Cross-sections of 5 MW designs of (a) the 8-pole generator of [1] and (b) the 10-pole generator of [2].

This work was financially supported by the Centre for Renewable and Sustainable Energy Studies at Stellenbosch University in South Africa and the Department of Science and Innovation (DSI) in South Africa.

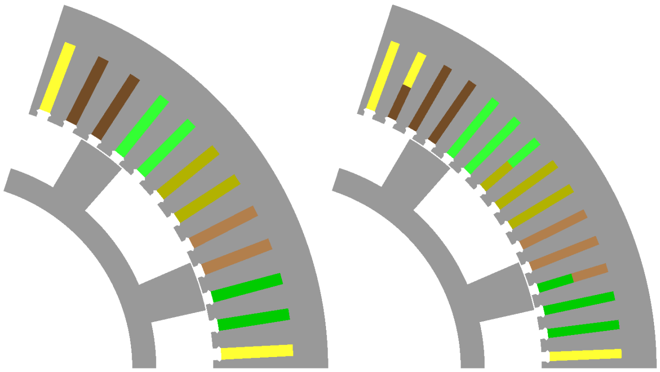

(a) (b)

Fig. 2. Cross-sections of simple salient-pole 5 MW RSG designs with (a) an integral-slot (60 slots) winding and (b) a fractional-slot (75 slots) winding.

rotor of the style show in Fig. 2. This process results in the creation of various alternative salient-pole machines that are still comparatively simple to manufacture and mechanically robust. These alternative designs are individually optimised in an effort to improve upon the performance of the baseline, simple salient-pole machine.

Lastly, in order to compare the performance of the RSGs in this paper to [2], the design of a 10-pole, 5 MW, 500 r/min RSG wind generator is again considered here, with the RSG volume constrained to that of [2]. A lower current density of less than J = 2 A/mm^2 and an electrical loading less than A = 80 kA/m, in order to have feasible AJ values, are used in the design in order to enable air cooling. A higher fill factor of 0.6, which is consistent with [9] and [10], is chosen. A slightly more conservative air gap of 3 mm is also implemented.

II. Modelling

In the modelling of the RSG, we use the classical dq analysis and dq equivalent circuits of Fig. 3. The flux linkages are calculated from rotor-step finite element (FE) analysis. The induced voltages, E_d and E_q, are accounted for in the equivalent circuit of Fig. 3. The effect of the core losses is incorporated in the equivalent circuits by means of the core loss resistance, R_c. The core losses, P_c, are calculated from a modified version of a Steinmetz's core loss equation and using FE-calculated tooth and yoke flux densities. The core loss resistance is then determined by

$$R_c = \frac{3(E_d^2 + E_q^2)}{2P_c} \tag{1}$$

The effect of the end winding inductance, L_e, is also incorporated into the equivalent circuits, as shown by the end winding induced voltages in Fig. 3. The end winding inductance calculation is explained in [11]. The dq-voltage and -inductance equations are given by (2) to (5). The dq-voltages and -currents of the equivalent circuits are explained further in the phasor diagram in generator mode in Fig. 4, where θ is the current angle and ϕ the power factor angle.

$$V_d = R_s I_{d1} - \omega_e \lambda_q - L_e I_{q1} \omega_e \tag{2}$$

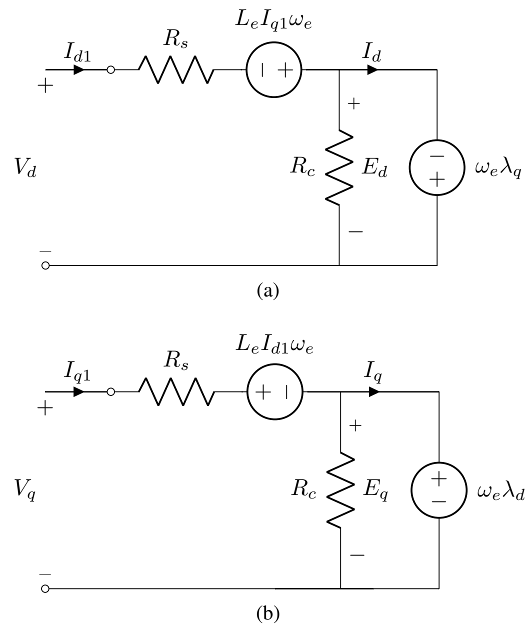

Fig. 3. DQ equivalent circuits.

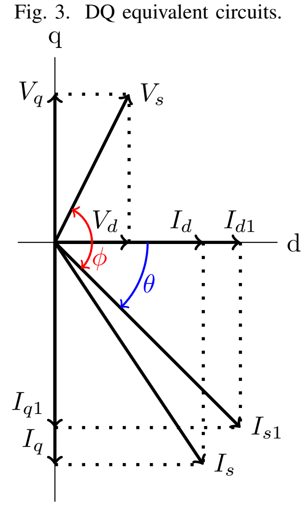

Fig. 4. Phasor diagram in generator mode.

$$V_q = R_s I_{q1} + \omega_e \lambda_d + L_e I_{d1} \omega_e \tag{3}$$

$$L_d = \lambda_d / I_d \tag{4}$$

$$L_q = \lambda_q / I_q \tag{5}$$

The torque of the RSG is calculated from the equivalent circuit modelling as

$$T_e = \frac{3}{4} p(\lambda_d I_q - \lambda_q I_d) = \frac{3}{8} p(L_d - L_q) \hat{I}_s^2 sin(2\theta), \tag{6}$$

where p is the number of poles. We also developed a simple torque equation for the specific machine structure of Fig. 2. The reason for this is to quickly verify the torque capability of the generator. Furthermore, the equation can be used for the initial sizing of such a generator.

To derive a simple torque equation, a capture of the air-gap flux density of the RSG under full load is used, as shown in Fig. 5. The averaged flux density waveform in Fig. 5 is further

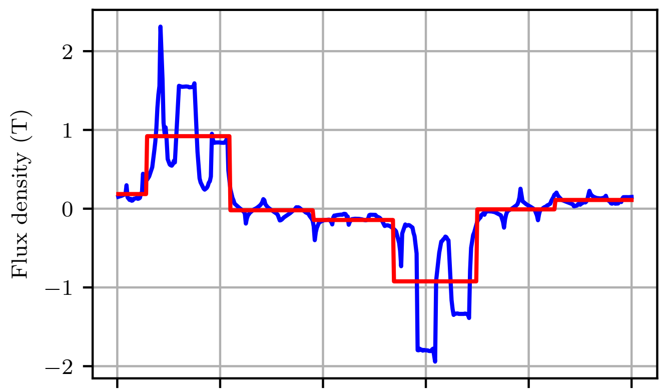

Fig. 5. Capture of actual and averaged air-gap flux density waveforms of the RSG under full load.

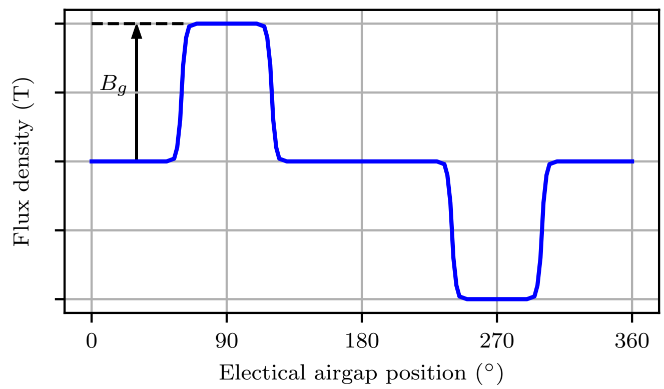

Fig. 6. Assumed air-gap flux density waveform of the RSG.

simplified to that shown in Fig. 6. With this simplification, the q-axis radial flux between the rotor poles is assumed to be zero.

In Fig. 6, B_g is the average peak-plateau flux density in the air-gap between the rotor pole and the stator core teeth. This flux density can be determined from FE or simple magnetic equivalent circuit analyses. Using the concept of the Lorenz force, a torque equation is derived in the Appendix similar to the torque derivation for brushed- and brushless DC machines, as

$$T_{e(2)} = \frac{1}{2} N_s B_g J_s A_{cu} k_f k_r k_A d_g l_s, \tag{7}$$

where N_s is the number of stator slots, k_r is an active slot factor and k_A a correction factor for chorded windings; these factors are defined in the Appendix. Further in (7), J_s is the RMS stator current density, A_{cu} is the copper area of the slot, k_f is the stator slot fill factor, d_g is the air-gap diameter and l_s is the stack length of the core.

By means of the above modelling, the performance of the generator in terms of power factor, torque and efficiency is determined. This performance calculation is used in the design optimisation of the RSG discussed in Section IV and applied in Section V.

III. Finite Element Simulation

The RSG is simulated using an in-house FE-method package called *SEMFEM* [12]. The accuracy of this package is evaluated against the calculated results of the commercial *Ansys Maxwell* FE package. In this section we consider, in particular, the effect of the stator winding and skewing on the torque quality of the RSG.

A. Integral- versus Fractional-Slot Windings

Fig. 7 shows the torque versus rotor position of the unskewed, 5 MW RSG, using the integral-slot winding of Fig. 2a. The integral-slot winding results in an immense torque ripple, which is generally a challenge for RSGs. Fairly good agreement is found in the calculated torque results of *SEMFEM* and *Maxwell* for this high torque ripple case, as shown in Fig. 7. As shown by [13], a fractional-slot winding can be effective in decreasing the torque ripple of reluctance synchronous machines. Fig. 7 illustrates this decrease in the torque ripple of the RSG in Fig. 2(b), with its fractional-slot winding, remarkably well.

B. Rotor Skewing

Another method proven to decrease torque ripple in RSGs is rotor skewing, as demonstrated in [14] and [15]. The influence of rotor skewing on the torque ripple of the simple salient-pole RSG is shown in Table I. The torque ripple of the optimised and skewed RSG of Fig. 8 decreases to below 5 %, and is in strong contrast with the unskewed machines of Fig. 2.

The skewing process has been thoroughly illustrated by [3] and [15], but is described here briefly. First, a skew angle is chosen. A larger skew angle can offer a larger reduction in torque ripple, but also results in a reduction in machine performance. A skew angle of a single slot pitch is regarded as conventional. However, by performing optimisations for the simple salient-pole RSG at a skew angle of one slot pitch and

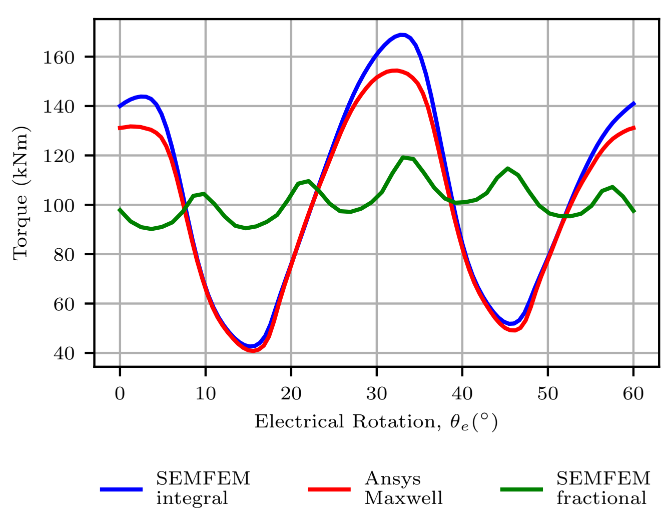

Fig. 7. A comparison of two FEM packages simulating the integral wound RSG of Fig. 2a, contrasted with the fractionally wound RSG of Fig. 2b.

TABLE I
TORQUE RIPPLE OF SKEWED AND UNSKEWED SALIENT-POLE RSGS WITH DIFFERENT STATOR WINDINGS

Unskewed		Skewed
Integral (Fig. 2a)	Fractional (Fig. 2b)	Fractional (Fig. 8)
123.6 %	28.64 %	4.74 %

two slot pitches respectively, it was found that a skew angle of two slot pitches results in a better optimum machine. The optimized, two slot pitch skewed RSG has a torque ripple lower than 5 % and offers better performance than an optimum machine skewed by only a single slot pitch, with the same 5 % torque ripple requirement. A skew angle of two slot pitches is hence selected.

In the FE analysis, the RSG is axially divided into five sub-machines, each relatively displaced by a fifth of the skew angle. In [14] it is found that five sub-machines are sufficient to represent continuous skew. If the skew angle is α, the positional rotation of the five sub-machines is given by,

$$\left[-2\frac{\alpha}{5}; -\frac{\alpha}{5}; 0; \frac{\alpha}{5}; 2\frac{\alpha}{5}\right]. \tag{8}$$

Each sub-machine is then simulated with their initial rotor positions altered by (8). The current angle for each sub-machine is also modified based on (8) by adding the displacement, converted to electrical degrees, to each current angle for every sub-machine simulation. The performance of the total RSG is then determined by averaging the simulation results of the five sub-machines for final performance calculations.

IV. DESIGN OPTIMISATION PROCESS

The optimisation process is handled with a commercial optimisation package called *VisualDOC*. *VisualDOC* iteratively interacts with the inputs and outputs of a *Python* script that is used to run the *SEMFEM* simulation. A single objective optimisation is used to find the optimum machine.

The objective is to maximize the power factor while constraining the power output to 5 MW, the efficiency to 98 % and the torque ripple to less than 5 %. The optimisation method that is used is a combination of the genetic algorithm, NSGA-II (non-dominated sorting genetic algorithm), and a gradient based algorithm, SLP (sequential linear programming).

To save time, the more resource-intensive NSGA-II algorithm is run first and, at a certain point, when the improvement in consecutive iterations becomes less pronounced, the best NSGA-II solution is used as the initial conditions for a less resource-intensive SLP optimisation. This strategy consistently resulted in a better optimum machine in a shorter time than simply using either of the optimisations methods individually. Between seven and nine optimisation parameters are optimised for every RSG design.

V. SALIENT-POLE RSG DESIGNS

Based on the aforementioned simulation and optimisation strategy, a series of optimisations are done for various RSGs that are all slightly different from one another. In all these designs the stator outer diameter (1.89 m) and stack length (1.89 m) of the machines are the same as in [2]. The performance results of the design optimisations are displayed in Table II, and the rationale for the different designs is discussed in this section.

TABLE II
PERFORMANCE SUMMARY AND COMPARISON OF SALIENT-POLE RSGS

Parameter	Unit	Baseline	Taper	Chamfer	Slit
Power out	[MW]	5.023	5.01	5.02	4.88
Power factor		0.539	0.543	0.541	0.538
Efficiency	[%]	97.94	97.90	97.87	97.86
Torque average	[kNm]	97.94	97.67	98.02	95.22
Torque ripple	[%]	4.74	4.82	4.88	5.62

A. Baseline salient-pole RSG

An optimum baseline salient-pole RSG is found by optimising the design parameters illustrated in Fig. 8. A description of all the design parameters in this section can be found in Table III. The performance of such a simple machine, before any modifications to the rotor, is already quite surprising. Yet the power factor is still quite low. The simple salient-pole RSG is subsequently subjected to further minor modifications in an effort to improve the power factor.

B. Tapered RSG

A rotor with tapered poles can be found in other non-permanent magnet rotors, such as the SRM [16] or the WF-FSG [17]. This rotor topology and its distinguishing optimisation parameters are illustrated in Fig. 9. The significant difference between the tapered RSG and the simple salient-pole RSG is an additional parameter that enables the pole to taper by increasing or decreasing dimension *R_pb*. This means that dimension *R_pl* would typically not be in line, radially, with the shaft center point, while the *R_pl* dimension of the baseline salient-pole RSG always proceeds radially from the shaft center. It was found that this rotor design slightly

TABLE III
DIMENSIONS OF THE SALIENT-POLE RSGS

Var	Description	Simple [mm]	Taper [mm]	Chamfer [mm]	Slit [mm]
S_yt	Stator yoke thickness	74.06	73.43	79.03	72.10
S_tw	Stator tooth width	16.06	16.01	15.15	15.37
S_tl	Stator tooth length	149.5	147.7	152.9	150.3
R_yt	Rotor yoke thickness	163	119.1	83	110.7
R_pw	Rotor pole width	143.4	143	188.8	143.4
R_pl	Rotor pole length	181.4	244.5	235.8	277
R_pb	Rotor pole base	115.1	86.3	86	118.7
R_sw	Rotor slit width	-	-	-	9.97
R_sl	Rotor slit length	-	-	-	219.5
R_cw	Rotor chamfer width	-	-	24.97	-
R_cl	Rotor chamfer length	-	-	200.6	-
R_ir	Rotor inner radius	374	357.2	391.3	442.6
R_or	Rotor outer radius	718.50	720.8	710.1	719.6

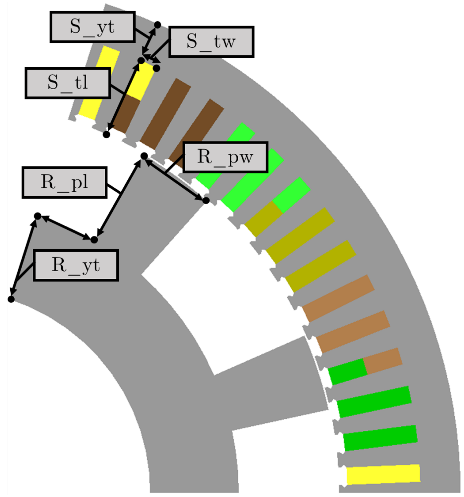

Fig. 8. Optimisation structure and parameters of the baseline salient-pole RSG.

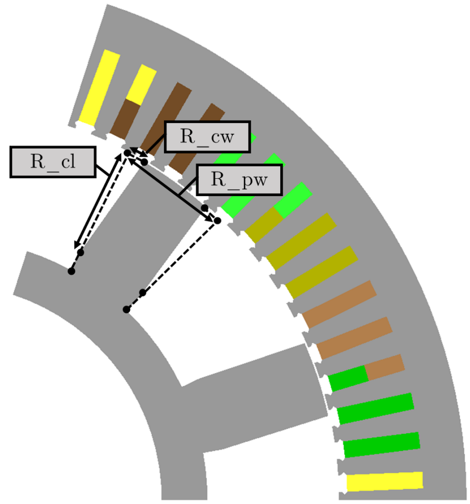

Fig. 10. Optimisation structure and parameters of the chamfered RSG.

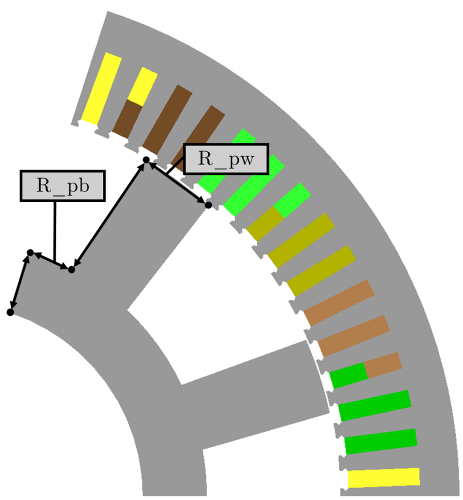

Fig. 9. Optimisation structure and parameters of the tapered RSG.

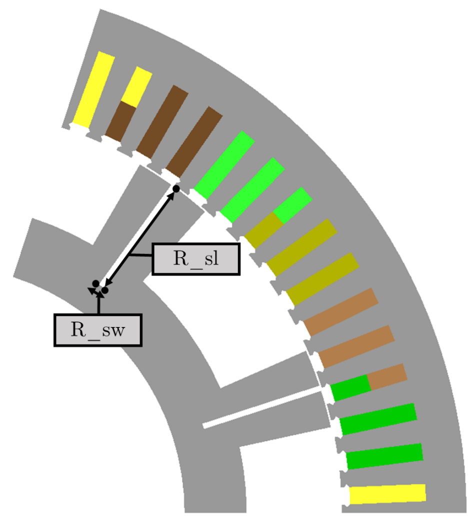

Fig. 11. Optimisation structure and parameters of the slitted RSG.

improved the power factor without negatively impacting other performance parameters.

C. Chamfered RSG

It is seen in [18] that chamfering the rotor poles of a multi-phase reluctance machine yields a slight improvement in performance. This is put to the test in a design optimisation with distinguishing optimisation variables, as in Fig. 10, allowing a type of chamfering to take place. The optimisation tends to make the chamfer quite large by increasing R_cl, in effect resembling the tapered RSG.

When the chamfering is much more constrained in an attempt to force the optimisation into a design that resembles [18], the optimum machine tends to have little, to no chamfering present. This indicates that the chamfering has little to no effect on the salient-pole RSG performance. Although the chamfered RSG in Fig. 10 (resembling the tapered RSG) shows slight improvement over the simple salient-pole RSG in Fig. 8, it does not show more improvement than the tapered RSG. A further attempt to chamfer only one side of the rotor pole, in order to potentially benefit from asymmetry, also does not result in any improvement.

D. Slitted RSG

It is also found in [18] that adding slits in the rotor pole of a multi-phase reluctance machine yields a slight improvement in performance. The idea is that slitting would minimize the q-axis flux and thus improve the saliency ratio and overall machine performance. Fig. 11 shows the distiniguishing design parameters for this rotor topology. It is telling that the optimisation consistently attempts to decrease the slit size, by decreasing R_sw, until the slit becomes insignificantly small. When the slit size is constrained in order to keep it from being too small, the slitted RSG's performance did not improve compared to the other salient-pole RSGs. This was tested for an optimisation with a single slit, as well as an optimisation with two variably spaced slits in the rotor pole.

VI. Optimum Design Assessment and Comparison

The optimum dimensions of the four optimally designed RSGs are given and explained in Table III. Of these dimensions, the air-gap diameter, but more particularly the rotor pole arc, are of interest. For all the RSGs, an optimum rotor pole arc of approximately 57° electrical is found. This is important information for the design engineer at initial design.

Based on the optimum performance results of Table II, the tapered salient-pole RSG is the design choice that shows the most significant improvement compared to the baseline salient-pole RSG. Although this improvement is not exceedingly significant, tapering seems to be an adaptation worth adopting, as it will be similar to the baseline salient-pole RSG in terms of manufacturing and mechanical strength.

The performance of the tapered salient-pole RSG versus current angle is further evaluated in Fig. 12. As is shown, a current angle of 54.34° at full load gives the best compromise for good torque, power factor and efficiency, while still maintaining a torque ripple lower than 5 %. The performance of this RSG is further compared, in Table IV, with that of the classical flux barrier rotor RSG of [2].

It is worth noting that the tapered salient-pole RSG offers a similar torque density to this distributed flux barrier rotor RSG with an equivalent volume. The main difference is the much lower power factor, as expected of the tapered salient-pole rotor RSG. Finally, the developed analytical torque equation (7) is shown, in Table IV ($T_{e(2)}$), to predict a slightly too high torque, which is as expected, but reasonably close for a first estimation.

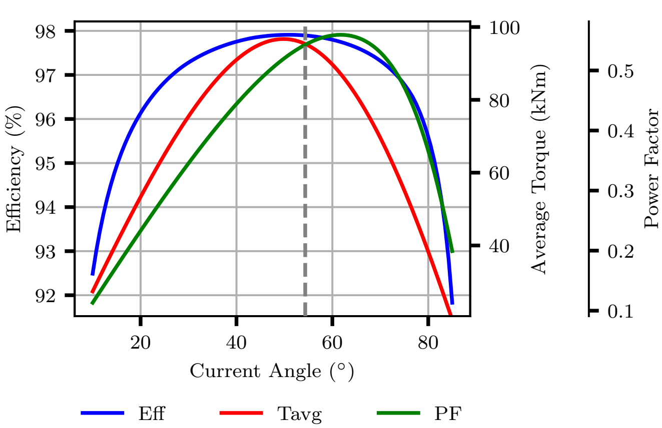

Fig. 12. Performance of the tapered salient-pole RSG in Fig. 9

VII. Conclusions and Future Work

A simple, mechanically-robust rotor structure is considered in this paper in the design of a 5 MW, 10-pole RSG wind generator. The following conclusions are drawn from the results.

TABLE IV
Comparison of RSGs in Fig. 1b and Fig. 9

		RSG of [2]	Tapered RSG
Power out	[MW]	5.05	5.01
Torque average	[kNm]	98.4	97.67
Torque $T_{e(2)}$	[kNm]	-	108
Efficiency	[%]	98.0	97.90
Power factor		0.853	0.543
Torque ripple	[%]	-	4.82
Poles		10	10
Slots per pole		9	7.5
Fill factor		0.35	0.6
Stator diameter	[m]	1.89	1.89
Stack length	[m]	1.88	1.89
Air gap	[mm]	2.5	3
Torque density	[kNm/m^3]	18.65	18.42
Current angle	[°]	73.4	54.34
Current density	[A/mm^2]	4.5	2
Speed	[r/min]	500	500
L_d	[mH]	-	151.6
L_q	[mH]	-	39.78
L_d/L_q	[mH]	-	3.81

With the proposed simple salient-pole rotor, together with realistic current densities and electric loads, the same torque densities and efficiencies surprisingly are obtained as that of the equivalent flux barrier rotor RSG of [2]. This is explained by the relatively small rotor pole, which drastically lowers the q-axis armature reaction and L_q inductance. However, the rotor pole is large enough to obtain a reasonable air gap flux density with a relatively high L_d inductance, so that the inductance difference and inductance ratio are relatively good.

It is shown that some simple modifications to the salient-pole rotor profile do not improve the performance of the RSG significantly. There is a slight improvement when adding an additional optimisation parameter to allow for the tapering of the rotor pole. Seeing as this design change does not dramatically influence the manufacturing process, it should be adopted.

With the proposed salient-pole rotor, the torque ripple of the RSG can be very large. However, fractional-slot windings, together with skewed salient-poles, show that the percentage torque ripple can be reduced to within 5 %.

A new, classic torque equation derived for the salient-pole rotor RSG gives a fairly quick prediction of the torque capability of this RSG. Together with the findings of an optimum rotor pole arc of 57° electrical, this equation can be used in first, quick designs of the proposed rotor RSG.

The disadvantage of the proposed rotor RSG is its relatively low power factor, typically 0.54. This increases the MVA capability and cost of only the synchronous rectifier side of the power electronic converter (not the grid-tie inverter side). However, the very cheap proposed salient rotor of the RSG potentially compensates for this increased cost.

VIII. Appendix

From the Lorenz force law the torque of the RSG can be expressed as

$$T_e = \frac{d_g}{2} B_g l_s I_{TP}, \tag{9}$$

where I_{TP} is the total current in the magnetic field. The total current in the magnetic field is the total q-axis current in the magnetic field and can be derived as

$$I_{TP} = \pi d_g k_r \sqrt{2} A_{rms} \sin\theta, \tag{10}$$

where $k_r = \theta_r/\theta_s$ and where θ_r is the mechanical rotor pole pitch and $\theta_p = 2\pi/p$ is the magnetic pole pitch. In (10) A_{rms} is the RMS current loading which is given by

$$A_{rms} = \frac{J_s A_{cu} k_f N_s k_A}{\pi d_g}, \tag{11}$$

where k_A is a correction factor for chorded and fractional-slot windings given by

$$k_A = \frac{N_{s1}}{N_s}\left(1 - \frac{\sqrt{3}}{2}\right) + \frac{\sqrt{3}}{2} \approx 0.134\frac{N_{s1}}{N_s} + 0.866. \tag{12}$$

In (11), N_{s1} is the number of those stator slots that have coil layers of the same phase. Replacing (10) and (11) into (9) and simplifying by assuming a current angle of $\theta = 45°$ we obtain

$$T_e = \frac{1}{2} B_g l_s d_g N_s A_{cu} k_f k_r k_A J_s. \tag{13}$$

References

[1] P. Roshanfekr, S. Lundmark, T. Thiringer, and M. Alatalo, "A synchronous reluctance generator for a wind application-compared with an interior mounted permanent magnet synchronous generator," in *7th IET International Conference on Power Electronics, Machines and Drives (PEMD 2014)*, pp. 1–5, April 2014.

[2] E. Howard and M. J. Kamper, "Reluctance synchronous wind generator design optimisation in the megawatt, medium speed range," in *2017 IEEE Energy Conversion Congress and Exposition (ECCE)*, pp. 1864–1871, Oct 2017.

[3] J. Dippenaar and M. J. Kamper, "A robust 5 MW split-pole reluctance synchronous wind generator," in *2020 XXIV International Conference on Electrical Machines (ICEM)*. in press.

[4] V. Yaramasu, B. Wu, P. C. Sen, S. Kouro, and M. Narimani, "High-power wind energy conversion systems: State-of-the-art and emerging technologies," *Proceedings of the IEEE*, vol. 103, pp. 740–788, May 2015.

[5] T. Holzer and A. Muetze, "Full-size converter operation of large hydro power generators: Generator design aspects," in *2018 IEEE Energy Conversion Congress and Exposition (ECCE)*, pp. 7363–7368, Sep. 2018.

[6] S. Taghavi and P. Pillay, "A mechanically robust rotor with transverse-laminations for a synchronous reluctance machine for traction applications," in *2014 IEEE Energy Conversion Congress and Exposition (ECCE)*, pp. 5131–5137, Sep. 2014.

[7] E. Annie Elisabeth Jebaseeli and D. Susitra, "Performance analysis of various configurations of switched reluctance machine for wind energy applications," in *Recent Advances in Space Technology Services and Climate Change 2010 (RSTS CC-2010)*, pp. 419–423, 2010.

[8] U. B. Akuru and M. J. Kamper, "Performance comparison of optimum wound-field and ferrite PM flux switching machines for wind energy applications," in *2016 XXII International Conference on Electrical Machines (ICEM)*, pp. 2478–2485, 2016.

[9] L. Sethuraman, M. Maness, and K. L. Dykes, "Optimized generator designs for the DTU 10-MW offshore wind turbine using generatorse: Preprint," in *American Institute of Aeronautics and Astronautics 35th Wind Energy Symposium*, 2017.

[10] Ion Boldea and Syed A. Nasar, *The Induction Machine Handbook*. CRC Press, 2002.

[11] M. J. Kamper, *Design Optimisation of Cageless Flux Barrier Rotor Reluctance Synchronous Machine*. Phd, Stellenbosch University, South Africa, 1996.

[12] S. Gerber, J. M. Strauss, and P. J. Randewijk, "Evaluation of a hybrid finite element analysis package featuring dual air-gap elements," in *The XIX International Conference on Electrical Machines - ICEM 2010*, pp. 1–6, 2010.

[13] V. A. Dmitrievskii, V. A. Prakht, and V. M. Kazakbaev, "Ultra premium efficiency (IE5 energy-efficiency class) synchronous reluctance motor with fractional slot winding," in *2018 XIII International Conference on Electrical Machines (ICEM)*, pp. 1015–1020, Sep. 2018.

[14] X. B. Bomela and M. J. Kamper, "Effect of stator chording and rotor skewing on performance of reluctance synchronous machine," *IEEE Transactions on Industry Applications*, vol. 38, pp. 91–100, Jan 2002.

[15] T. Hubert, M. Reinlein, A. Kremser, and H. Herzog, "Torque ripple minimization of reluctance synchronous machines by continuous and discrete rotor skewing," in *2015 5th International Electric Drives Production Conference (EDPC)*, pp. 1–7, Sep. 2015.

[16] G. K. Ptakh, D. A. Zvezdunov, and R. R. Mustafaev, "Selection of stator yoke height of traction switched reluctance motor," in *2016 2nd International Conference on Industrial Engineering, Applications and Manufacturing (ICIEAM)*, pp. 1–4, 2016.

[17] U. B. Akuru and M. J. Kamper, "Novel experimentation of a 10 kW geared medium-speed wound-field flux switching wind generator drive," in *2018 IEEE Energy Conversion Congress and Exposition (ECCE)*, pp. 6492–6498, 2018.

[18] E. T. Rakgati, M. J. Kamper, and A. D. Le Roux, "Torque performance of optimally designed six-phase reluctance DC machine," in *Conference Record of the 2006 IEEE Industry Applications Conference Forty-First IAS Annual Meeting*, vol. 3, pp. 1186–1192, 2006.